Journal of Power Sources 190 (2009) 596–600

Contents lists available at ScienceDirect

Journal of Power Sources

journal homepage: www.elsevier.com/locate/jpowsour

Short communication

Incorporation of polyaniline into macropores of three-dimensionally ordered macroporous carbon electrode for electrochemical capacitors

Sang-Wook Woo [a], Kaoru Dokko [b,*], Hiroyuki Nakano [a], Kiyoshi Kanamura [a]

[a] Department of Applied Chemistry, Tokyo Metropolitan University, 1-1 Minami-ohsawa, Hachioji, Tokyo 192-0397, Japan
[b] Department of Chemistry and Biotechnology, Yokohama National University, 79-5 Tokiwadai, Hodogaya-ku, Yokohama 240-8501, Japan

ARTICLE INFO

Article history:
Received 14 November 2008
Accepted 16 January 2009
Available online 30 January 2009

Keywords:
Electrochemical capacitors
Colloidal crystal template
Macroporous carbon
Polyaniline

ABSTRACT

Three-dimensionally ordered macroporous (3DOM) carbons having walls composed of mesosized spherical pores were prepared by a colloidal crystal templating method. A composite electrode consisting of bimodal porous carbon and polyaniline (PAn) was prepared by electropolymerization of aniline within the macropores of the bimodal porous carbon. It was found that the deposition of PAn decreased the porosity and specific surface area (SSA) of the electrode. The electrochemical properties of the composite electrode were characterized in a mixed solution of ethylene carbonate (EC) and diethyl carbonate (DEC) containing 1 mol dm^{-3} $LiPF_6$. The discharge capacity of the carbon–PAn composite electrode was 111 mAh $g_{carbon-PAn}{}^{-1}$ in the potential range of 2.0–4.0 V *vs.* Li/Li^+, which corresponded to a volumetric discharge capacity of 53 mAh cm^{-3}. Both the double-layer capacity (30 mAh g^{-1}) and the redox capacity of PAn (81 mAh g^{-1}) contributed to the discharge capacity of the composite electrode. The carbon–PAn composite showed good rate capability, and the discharge capacity at a high current density of 6.0 A g^{-1} was as high as 81 mAh g^{-1}.

1. Introduction

Electrochemical capacitors attract much attention due to their high capacitance, and there have been many attempts to utilize electrochemical capacitors in high power applications such as hybrid power systems for electric vehicles [1]. In the case of electric double-layer capacitors (EDLCs), the charge is accumulated at the interface between the electrode and electrolyte without accompanying electrochemical reactions, and activated carbon is used as the EDLC electrode material because of its high specific surface area (SSA) [2]. It is possible to charge and discharge the EDLCs at very high rates, because it is a non-Faradaic process. Moreover, the charge–discharge cycle life of an EDLC is very long; however, the energy densities of EDLCs are very low compared with lithium-ion batteries [3,4]. Therefore, there have been many recent reports of composite materials consisting of an electrochemically active material and porous carbon [5–13]. The discharge capacity of a porous electrode can be increased using the redox capacity (pseudo-capacity) of an active material. For example, several groups have reported the preparation of composite electrodes composed of porous carbon and electrically conducting polymers [5–8].

Porous electrodes consisting of carbon particles, a polymer binder, and conductive agent have been used to increase the electrochemical interface of electrochemical capacitors [2,3]. The electrode materials and electrode structure have been intensively studied for the improvement of the energy density and power density of energy storage devices [14–18]. In these electrochemical energy storage devices, electrochemical processes take place at the interface of the electrode and electrolyte, and the charge–discharge rate capability is strongly dependent on the nature of the interface. A large electrochemical interface is favorable to increase the power density of energy storage devices; therefore, the characteristics of the porous electrodes, such as the SSA, porosity, and pore size distribution (PSD), are key parameters used to determine the performance of electrochemical devices.

One interesting technology used to fabricate porous materials is the colloidal crystal templating method [19,20]. Three-dimensionally ordered macroporous (3DOM) materials can be prepared by this method, and these materials have been intensively studied in various fields [21–26]. 3DOM carbon has a 3D network path for electronic conduction and high porosity of more than 70%. Recently, we successfully prepared 3DOM carbon with walls composed of mesosized pores [26–29]. This bimodal porous carbon has a high specific surface area of more than 1000 m^2 g^{-1} due to the mesopores. In this study, a composite electrode consisting of bimodal porous carbon and polyaniline (PAn) was prepared by the electropolymerization of aniline within the macropores of bimodal

* Corresponding author. Tel.: +81 45 339 3942; fax: +81 45 339 3942.
E-mail address: dokko@ynu.ac.jp (K. Dokko).

0378-7753/$ – see front matter © 2009 Elsevier B.V. All rights reserved.
doi:10.1016/j.jpowsour.2009.01.050

porous carbon. The electrochemical properties of the composite electrode were examined as a positive electrode for an electrochemical capacitor in a non-aqueous electrolyte. PAn is an electrically conducting polymer, and the redox reaction of PAn is accompanied by the insertion/deinsertion of counter ions [30]. The strategy of this research is to use the macropores as a space for the incorporation of an active material. In addition, the formation of an electric double-layer at the surface of the porous carbon mesopores can deliver a capacity. From the combination of the redox capacity of the active material and the electric double-layer capacity of the bimodal porous carbon, a large discharge is anticipated for the composite electrode.

2. Experimental

Bimodal porous carbon, that is, 3DOM carbon with walls composed of spherical mesopores, was prepared by the colloidal crystal templating method [27]. Polystyrene (PS) latex and colloidal silica were utilized to prepare the colloidal crystal templates for the bimodal porous carbon. PS particles (Seradyn Inc.) with a diameter of 204 nm were utilized as the template for the macropores, and colloidal silica (Snowtex®, Nissan Chemical Industries Ltd.) with a diameter range of 10–20 nm was used as the template for the mesopores. Mono-dispersed PS latex and the colloidal silica particles were uniformly mixed in deionized water by ultrasonic treatment. The water in the mixed suspension was simply evaporated from a Petri dish at 333 K for 24 h, leaving the PS–silica composite accumulated at the bottom of the Petri dish. The volume ratio of PS to silica in the composite was controlled at 74:26, which allowed the PS beads to form a close-packed lattice in the composite. The obtained PS–silica composites were treated at high temperatures in a horizontal furnace under dry argon flow (40 mL min^{-1}), in order to carbonize the PS beads. The temperature was increased from room temperature to 1273 K at a heating rate of 4 K min^{-1} and then reduced to room temperature. After carbonization, the silica particles were removed with 20% aqueous hydrofluoric acid, and the resulting porous carbons were washed with ultra pure water and dried in a vacuum oven at 383 K.

The porous carbon electrode was prepared by mixing bimodal porous carbon and polytetrafluoroethylene (PTFE) binder in a 90:10 (w/w). This mixture was rolled into a thin sheet of uniform thickness and then cut into a circular sheet with a diameter of 13 mm. The sheet was then pressed onto a titanium mesh current collector. The thickness of the sheet was 130–135 μm at this point, and the mass of the bimodal porous carbon in the sheet was 5.4 mg. Electrochemical polymerization of aniline on the porous carbon electrode was conducted using a cyclic potential sweep in a propylene carbonate (PC) solution containing 1.0 mol dm^{-3} $LiClO_4$, 2.0 mol dm^{-3} CF_3COOH, and 0.5 mol dm^{-3} aniline [31]. A conventional three-electrode cell was utilized for the polymerization, and Li/Li^+ (1 mol dm^{-3} $LiClO_4$ in PC) and an activated carbon electrode (KYNOL™, BET-SSA: 2000 m^2 g^{-1}) were used as the reference and counter electrodes, respectively. The prepared composite electrode was rinsed in ethanol to remove aniline monomer, and dried under vacuum at 363 K for 24 h. The composite electrode is hereafter denoted as carbon–PAn (*x*) (*x*: content of PAn), for example, carbon–PAn (40) represents a composite composed of 60 wt.% carbon and 40 wt.% PAn.

The porous structure of the composite electrode was observed using a field-emission scanning electron microscope (FE-SEM; JSM 6700F, JEOL). Nitrogen (N_2) adsorption–desorption measurements were conducted at 77 K using a porosimetry analyzer (Belsorp-mini II, BEL Japan, Inc.). The specific surface area (S_{BET}) was calculated from the Brunauer–Emmett–Teller (BET) plot of the nitrogen adsorption isotherm. The PSD and average pore diameter (D_{BJH}) in the range of 2–50 nm were calculated using the Barret–Joyner–Halenda (BJH) method with the adsorption curve of the N_2 isotherm [32]. The surface area (S_{micro}) and pore volume (V_{micro}) of the micropores of the prepared carbon and composite were estimated by the *t*-plot method [33].

A standard three-electrode electrochemical cell was assembled to measure the specific capacity of the carbon–PAn composite electrode. The counter electrode used was activated carbon fiber, and Li/Li^+, $LiClO_4$ (1 mol dm^{-3} $LiClO_4$ in PC) was used as the reference electrode. A mixed solution of ethylene carbonate (EC) and diethyl carbonate (DEC) (1:1, v/v) containing 1.0 mol dm^{-3} $LiPF_6$ was used as the electrolyte. Cyclic voltammetry was carried out using an automatic polarization system (HZ-100R, Hokuto Denko). Galvanostatic discharge–charge tests were performed using an automatic discharge–charge instrument (HJR-110mSM6, Hokuto Denko). All electrochemical measurements were carried out in an argon-filled glove box at room temperature.

3. Results and discussion

Fig. 1 shows FE-SEM images of the prepared bimodal porous carbon. The mechanism for the formation of the bimodal porous structure has been reported elsewhere [27]. During the evaporation of water in the mixed suspension of PS and silica, the mono-dispersed PS beads are self-assembled into an ordered lattice, wherein the silica particles are forced to pack closely at the interstices between the PS beads [27–29]. Heat treatment of the PS–silica composite creates 3D-ordered macropores due to the decomposition of PS, and simultaneously, some fragments of the decomposing polymer deposit are formed around the silica colloids. Finally, the silica particles are removed by HF etching to form mesopores, and bimodal porous carbon is obtained. The prepared carbon had an inverse opal structure, and the macropore size (190 nm) was slightly smaller than the size of the PS beads (204 nm) used as the macropore templates. This is probably due to the shrinkage of the macropore during the carbonization process. As shown in Fig. 1, the walls of the macropores are composed of spherical mesopores with sizes of 10–20 nm, which is in good agreement with the size of the silica particles used as the mesopore templates.

Electrochemical polymerization of aniline on the bimodal porous carbon was conducted in a PC solution containing aniline and CF_3COOH by cyclic potential sweep between 2.4–3.8 V *vs.* Li/Li^+ at a scan rate of 10 mV s^{-1}. Fig. 2 shows cyclic voltammograms (CVs) of porous carbon in the PC solution containing aniline. At the first cycle, a large anodic current was observed at above 3.6 V *vs.* Li/Li^+,

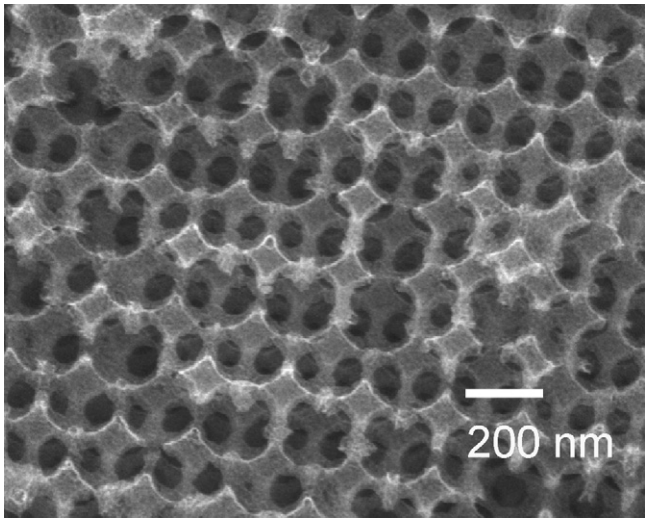

Fig. 1. FE-SEM images of bimodal porous carbon.

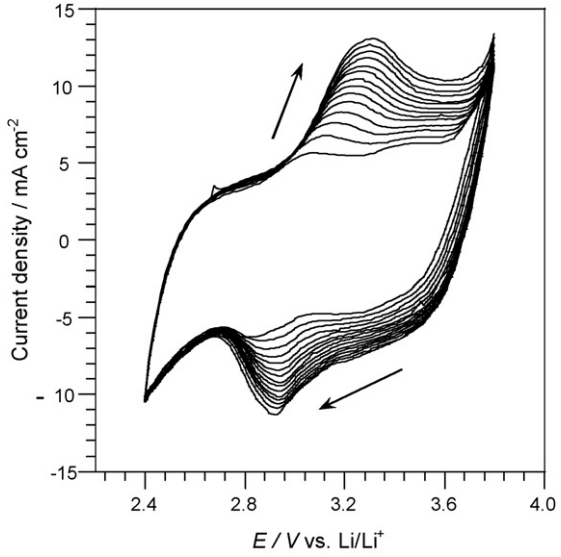

Fig. 2. Cyclic voltammograms of a bimodal porous carbon electrode in a PC solution containing 1.0 mol dm^{-3} $LiClO_4$, 2.0 mol dm^{-3} CF_3COOH, and 0.5 mol dm^{-3} aniline. The potential sweep rate was 10 mV s^{-1}, and was carried out for 15 successive cycles.

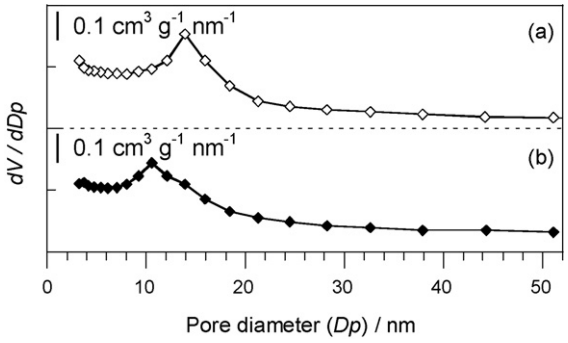

Fig. 4. Pore size distributions of (a) bimodal porous carbon and (b) carbon–PAn composite (42.1 wt.%).

indicating the formation of reactive anilinium radical cations by the electrochemical oxidation of aniline in the presence of the highly acidic CF_3COOH proton source. This leads to the polymerization of aniline involving the coupling of anilinium radical cations [31,34]. As the cycle number increased, the redox current for doping and undoping of ClO_4^- to polyaniline appeared at around 3.1 and 2.9 V, respectively, and the redox peaks were increased [34–36]. Fig. 3 shows SEM images of the carbon–PAn composite electrodes. PAn was deposited on the surface of the macropores, and the porosity of the carbon gradually decreased with increasing cycle number. After 30 potential sweep cycles, PAn occupied most of the macropores in the porous carbon, which resulted in the blockage of the connecting windows between the macropores. The amount of deposited PAn in the composite after 30 cycles was approximately 48 wt.%.

The PSD of bimodal porous carbon is displayed in Fig. 4(a), indicating that the bimodal porous carbon has mesopores ranging from 10 to 20 nm. The mesopore size centered at around 12 nm is in good agreement with the template silica particle size (10–20 nm diameter). The increase in pore volume corresponding to a pore size of around 2 nm is probably due to the interstitial spaces between the spherical mesopores. Fig. 4(b) shows the PSD of the composite carbon–PAn (42). The deposition of PAn resulted in the decrease of the mesopore peak diameter, indicating the partial filling of the bimodal porous carbon mesopores with PAn. However, it should be noted that the mesopores of the porous carbon are not closed after the deposition of PAn. The open-mesopores can therefore contribute to the double-layer formation during charging and discharging of the electrode in an electrolyte. The pore characteristics of the bimodal porous carbon and carbon–PAn composite are summarized in Table 1. The BET-SSA (S_{BET}) of bimodal porous carbon was found to be 1001 m^2 g^{-1}. The surface area due to micropores (<2 nm), estimated using the *t*-plot method, was less than 10% of the

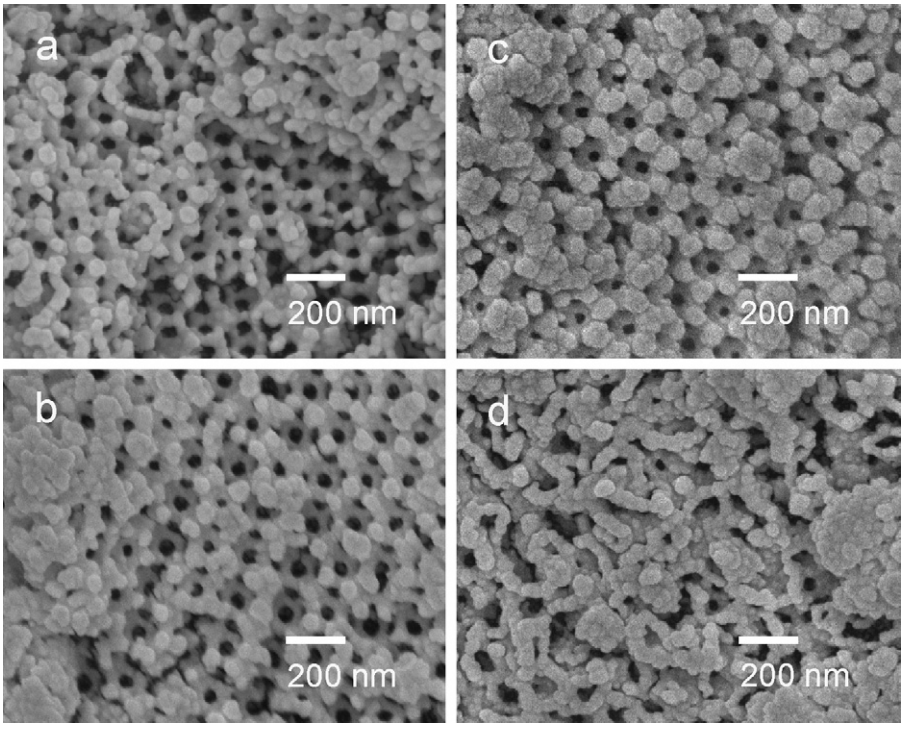

Fig. 3. FE-SEM images of composite electrodes consisting of bimodal porous carbon and PAn. The PAn contents in the composite electrodes were (a) 31.8 wt.%, (b) 38.7 wt.%, (c) 42.1 wt.%, and (d) 48.3 wt.%.

Table 1
Pore characteristics of bimodal porous carbon and the carbon–PAn (42.1 wt.%) composite.

Item	Specific surface areas ($m^2\ g^{-1}$)			Pore diameter (nm)		Pore volume ($cm^3\ g^{-1}$)	
	S_{BET}[a]	S_{micro}[b]	S_{ext}[c]	D_{BJH}[d]	D_{macro}[e]	V_{total}[f]	V_{micro}[g]
Bimodal porous carbon	1001	57	946	14	190	2.93	0.021
carbon–PAn (42.1 wt.%)	624	63	561	11	–	1.73	0.023

[a] S_{BET}: BET surface area.
[b] S_{micro}: Micropore surface area calculated from *t*-plot method.
[c] S_{ext}: External surface area; ($S_{ext} = S_{BET} - S_{micro}$).
[d] D_{BJH}: average pore diameter calculated from BJH method.
[e] D_{macro}: Pore diameter estimated from SEM observation.
[f] V_{total}: Total pore volume at a relative pressure of 0.99.
[g] V_{micro}: Micropore volume calculated from *t*-plot method.

BET-SSA. Therefore, the surface area of porous carbon is mostly due to both mesopores and macropores. On the other hand, the BET-SSA of the carbon–PAn composite was approximately 624 $m^2\ g^{-1}$. The introduction of PAn into bimodal porous carbon resulted in a significant decrease of the SSA and the total pore volume (V_{total}).

Fig. 5 presents the CVs of carbon–PAn composite electrodes in 1 mol dm^{-3} $LiPF_6$ (EC–DEC) at a scan rate of 5 mV s^{-1}. The initial potentials (immersion potentials of the electrodes) of bare porous carbon and carbon–PAn were between 3.0 and 3.3 V *vs.* Li/Li^+. The bare porous carbon electrode had a rectangular-like shape, which corresponds to the typical voltammogram profile of a double-layer capacitor [2]. From the shape of the CV curve for bare porous carbon, it is evident that Faradaic processes were not significantly involved in the potential range of 2.0–4.0 V *vs.* Li/Li^+. For the composite electrode consisting of porous carbon and PAn, besides the current response due to the formation of an electric double-layer, a redox current response was observed in the potential range of 2.5–4.0 V *vs.* Li/Li^+. In this potential region, aniline as an emeraldine salt (polaron formation) is oxidized and emeraldine is reduced to aniline during the anodic and cathodic scans, respectively [34–38]. Simultaneously, the insertion/deinsertion of PF_6^- anions into/from PAn takes place. The redox currents increased with the increase of the PAn content in the range of 0–40 wt.%. Despite the increased amount of PAn, the redox current of the composite electrode carbon–PAn (48) was smaller than that of carbon–PAn (42). For carbon–PAn (48), blockage of the connecting windows between macropores occurred during the electropolymerization process, as shown in Fig. 3(d), and this hindered ionic conduction within the composite electrode. This would lead to an increase of electrode resistance and a decrease in the utilization of PAn.

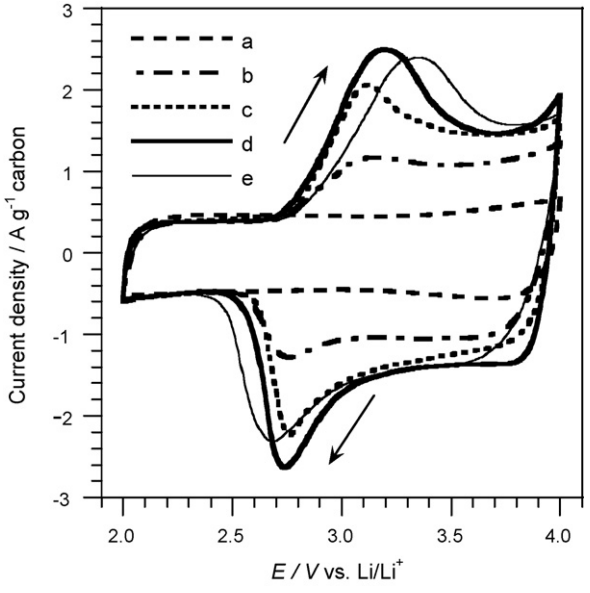

Fig. 5. Cyclic voltammograms of (a) bimodal porous carbon and (b–e) carbon–PAn composite electrodes measured at a scan rate of 5 mV s^{-1} in an electrolyte of 1 mol dm^{-3} $LiPF_6$/EC + DEC. The PAn contents in the composite electrodes were (b) 25.8 wt.%, (c) 38.7 wt.%, (d) 42.1 wt.%, and (e) 48.3 wt.%. The current of the cyclic voltammograms was normalized using the mass of bimodal porous carbon in the composite electrode.

Fig. 6 shows the charge and discharge curves for bare porous carbon and carbon–PAn (42) measured at a current density of 0.1 A g^{-1} in 1 mol dm^{-3} $LiPF_6$ (EC–DEC). The electrode potential of bare porous carbon changed linearly with the quantity of electricity passed for the charge and discharge processes. This can be attributed to the charge and discharge of the electric double-layer, and is in good agreement with the cyclic voltammetry results. In contrast, the charge and discharge curves of carbon–PAn (42) had an inflection at around 2.5 V *vs.* Li/Li^+. In the potential range of 2.0–2.5 V, charging and discharging of the double-layer occurred, while no significant Faradaic processes were apparent. Besides the double-layer formation, insertion/deinsertion of PF_6^- anions into/from PAn occurred in the potential range of 2.5–4.0 V *vs.* Li/Li^+. The discharge capacities of bare porous carbon and the carbon–PAn (42) composite measured at a current density of 0.1 A g^{-1} were 53 mAh g_{carbon}^{-1} and 111 mAh $g_{carbon-PAn}^{-1}$, respectively. Thus, the incorporation of PAn dramatically increases the charge storage capacity of the electrode. The discharge capacity of carbon–PAn (42) was attributed to the sum of the electric double-layer (30 mAh $g_{carbon-PAn}^{-1}$) and the redox capacity (81 mAh $g_{carbon-PAn}^{-1}$). The discharge capacity due to the redox reaction of PAn can be calculated as 198 mAh g_{PAn}^{-1} based on the mass of deposited PAn, which corresponds to a doping level of 0.6 electrons per aniline-unit [35,36]. A more important characteristic for the electrodes of electrochemical capacitors is the volumetric capacity. The volumetric capacity of the composite was found to be

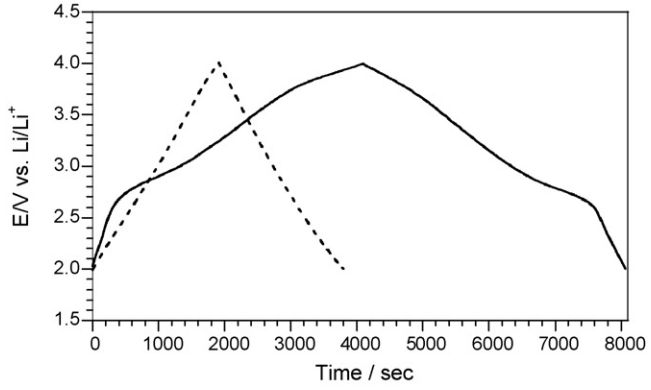

Fig. 6. Charge and discharge curves of bimodal porous carbon (dashed line) and the carbon–PAn (42.1 wt.%) composite electrode (solid line) measured at a current density of 0.1 A g^{-1} in an electrolyte of 1 mol dm^{-3} $LiPF_6$/EC + DEC.

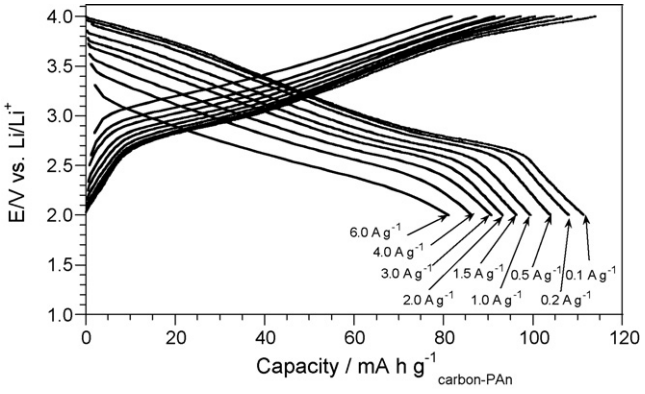

Fig. 7. Charge and discharge curves of the carbon–PAn (42.1 wt.%) composite electrode measured at various current densities.

53 mAh cm^{-3}, which is three times larger than that of bare porous carbon (16.5 mAh cm^{-3}). The porosity of bare bimodal porous carbon was more than 70%, and the incorporation of PAn into the macropores did not change the geometric volume of the carbon electrode. Therefore, this type of macroporous structure is suitable for the support of electrochemical active materials.

Fig. 7 shows the charge and discharge curves for carbon–PAn (42) measured at various current densities. The composite of carbon and PAn showed a good rate capability, and its discharge capacity at a high current density of 6.0 A g^{-1} (6.0 A g^{-1} corresponds to a current density of 21.0 mA cm^{-2}) was as high as 81 mAh g^{-1}, which is 73% of the discharge capacity of 111 mAh g^{-1} measured at a low current density of 0.1 A g^{-1}. The rate capability of carbon–PAn (42) in a non-aqueous electrolyte is good compared with those of electrically conducting polymer–carbon composite electrodes presented in the literature [39,40]. The high rate capability of the carbon–PAn composite can be attributed to facile doping (/undoping) processes in the composite electrode at the large interface between PAn and the electrolyte.

4. Conclusions

Bimodal porous carbon was prepared using a colloidal crystal templating method. A composite electrode consisting of bimodal porous carbon and PAn was prepared by electropolymerization of aniline within the macropores of the bimodal porous carbon. The deposition of PAn decreased the porosity of the electrode, and the optimum amount of PAn in the composite electrode that could deliver the maximum discharge capacity was 42 wt.%. The discharge capacity of the carbon–PAn composite electrode was 111 mAh $g_{carbon-PAn}^{-1}$ in the potential range from 2.0 and 4.0 V *vs.* Li/Li^+, which corresponds to the volumetric discharge capacity of 53 mAh cm^{-3}, and the double-layer capacity (30 mAh g^{-1}) and redox capacity of PAn (81 mAh g^{-1}) contributed to the discharge capacity of the composite electrode. It can be concluded that the incorporation of PAn into the macropores of bimodal porous carbon is effective in increasing the volumetric discharge capacity of the composite electrode. The composite of carbon and PAn showed a good rate capability, and its discharge capacity at a high current density of 6.0 A g^{-1} was as high as 81 mAh g^{-1}.

Acknowledgements

This work was partially supported by the Industrial Technology Research Grant Program in 2007 (07A22007a) from the New Energy and Industrial Technology Development Organization (NEDO) of Japan. The authors would like to thank Prof. H. Masuda and Dr. K. Nishio (Tokyo Metropolitan University) for their assistance in taking the FE-SEM micrographs.

References

[1] J.R. Miller, A.F. Burke, Electrochem. Soc. Interf. 17 (1) (2008) 53.
[2] B.E. Conway, Electrochemical Supercapacitors; Scientific Fundamentals and Technology Applications, Kluwer Academic/Plenum Publishers, New York, 1999.
[3] A. Burke, J. Power Sources 91 (2000) 37.
[4] A. Du Pasquier, I. Plitz, S. Menocal, G. Amatucci, J. Power Sources 115 (2003) 171.
[5] V. Khomenko, E. Frackowiak, F. Béguin, Electrochim. Acta 50 (2005) 2499.
[6] E. Frackowiak, V. Khomenko, K. Jurewicz, K. Lota, F. Béguin, J. Power Sources 153 (2006) 413.
[7] V. Gupta, N. Miura, Electrochim. Acta 52 (2006) 1721.
[8] M.J. Bleda-Martínez, C. Peng, S. Zhang, G.Z. Chen, E. Morallón, D. Cazorla-Amorósa, J. Electrocehm. Soc. 155 (2008) A672.
[9] T. Kudo, Y. Ikeda, T. Watanabe, M. Hibino, M. Miyayama, H. Abe, K. Kajita, Solid State Ion. 152–153 (2002) 833.
[10] H. Yamada, K. Tagawa, M. Komatsu, I. Moriguchi, T. Kudo, J. Phys. Chem. C 111 (2007) 8397.
[11] S.R. Sivakkumar, J.M. Ko, D.Y. Kim, B.C. Kim, G.G. Wallace, Electrochim. Acta 52 (2007) 7377.
[12] A.E. Fischer, K.A. Pettigrew, D.R. Rolison, R.M. Stroud, J.W. Long, Nano Lett. 7 (2007) 281.
[13] D. Bélanger, T. Brousse, J.W. Long, Electrochem. Soc. Interf. 17 (1) (2008) 49.
[14] H. Shi, Electrochim. Acta 41 (1996) 1633.
[15] S. Shiraishi, H. Kurihara, L. Shi, T. Nakayama, A. Oya, J. Electrochem. Soc. 149 (2001) A855.
[16] H. Zhou, S. Zhu, M. Hibino, I. Honma, J. Power Sources 122 (2003) 219.
[17] J. Chmiola, G. Yushin, Y. Gogotsi, C. Portet, P. Simon, P.L. Taberna, Science 313 (2006) 1760.
[18] C.-W. Huang, H. Teng, J. Electrochem. Soc. 155 (2008) A739.
[19] B.T. Holland, C.F. Blanford, A. Stein, Science 281 (1998) 538.
[20] A. Stein, R.C. Schroden, Curr. Opin. Solid State Mater. Sci. 5 (2001) 553.
[21] Z. Wang, F. Hu, P.K. Shen, Electrochem. Commun. 8 (2006) 1764.
[22] K.M. Shaju, P.G. Bruce, Adv. Mater. 18 (2006) 2330.
[23] M.W. Perpall, K.P.U. Perera, J. Dimaio, J. Ballato, S.H. Foulger, D.W. Smith Jr., Langmuir 19 (2003) 7153.
[24] J.H. Holtz, S.A. Asher, Nature 389 (1997) 7153.
[25] I. Moriguchi, F. Nakahara, H. Furukawa, H. Yamada, T. Kudo, Electrochem. Solid State Lett. 7 (2004) A221.
[26] H. Yamada, H. Nakamura, F. Nakahara, I. Moriguchi, T. Kudo, J. Phys. Chem. C 111 (2007) 227.
[27] S.W. Woo, K. Dokko, K. Sasajima, T. Takei, K. Kanamura, Chem. Commun. (2006) 4099.
[28] S.W. Woo, K. Dokko, H. Nakano, K. Kanamura, Electrochemistry 75 (2007) 635.
[29] S.W. Woo, K. Dokko, H. Nakano, K. Kanamura, J. Mater. Chem. 18 (2008) 1674.
[30] P. Novák, K. Muller, K.S.V. Santhanam, O. Hass, Chem. Rev. 97 (1997) 207.
[31] T. Osaka, T. Nakajima, K. Naoi, B.B. Owens, J. Electrochem. Soc. 137 (1990) 2139.
[32] E.P. Barrett, L.G. Joyner, P.P. Halenda, J. Am. Chem. Soc. 73 (1951) 373.
[33] F. Rouquerol, J. Rouquerol, K. Sing, Adsorption by Powders and Porous Solids: Principles, Methodology and Applications, Academic Press, London, 1999.
[34] J. Motheo, E.C. Venancio, L.H.C. Mattoso, Electrochim. Acta 43 (1998) 755.
[35] J. Desilvestro, W. Scheifele, O. Haas, J. Electrochem. Soc. 139 (1992) 2727.
[36] F. Fusalbe, D. Gouerec, D. Villers, D. Bélanger, J. Electrochem. Soc. 148 (2001) A1.
[37] T. Osaka, T. Nakajima, K. Shiota, T. Momma, J. Electrochem. Soc. 138 (1991) 2853.
[38] K. Kanamura, Y. Kawai, S. Yonezawa, Z. Takehara, J. Electrochem. Soc. 142 (1995) 2894.
[39] S.R. Sivakkumar, J.S. Oh, D.W. Kim, J. Power Sources 163 (2006) 573.
[40] S.R. Sivakkumar, D.W. Kim, J. Electrochem. Soc. 154 (2007) A134.